

# External magnetic field effects on a distorted kagome antiferromagnet

J.-H. Kim<sup>1</sup>, S. Ji<sup>1,2</sup>, S.-H. Lee<sup>1</sup>, B. Lake<sup>3,4</sup>, T. Yildirim<sup>2</sup>, H. Nojiri<sup>5</sup>, H. Kikuchi<sup>6</sup>, K. Habicht<sup>3</sup>, Y. Qiu<sup>2</sup>, and K. Kiefer<sup>3</sup>

<sup>1</sup>*Department of Physics, University of Virginia, Charlottesville, Virginia 22904*

<sup>2</sup>*NIST Center for Neutron Research, National Institute of Standards and Technology, Gaithersburg, Maryland 20899*

<sup>3</sup>*Hahn-Meitner-Institut, Glienicker Strabe 100, Berlin D-14109, Germany*

<sup>4</sup>*Institut für Festkörperphysik, Technische Universität Berlin, Hardenbergstr. 36, 10623 Berlin, Germany*

<sup>5</sup>*Institute for Materials Research, Tohoku University, Sendai, Miyagi 980-0821, Japan*

<sup>6</sup>*Department of Applied Physics, University of Fukui, Fukui 910-8507, Japan*

(Dated: October 26, 2018)

We report bulk magnetization, and elastic and inelastic neutron scattering measurements under an external magnetic field,  $H$ , on the weakly coupled distorted kagomé system,  $\text{Cu}_2(\text{OD})_3\text{Cl}$ . Our results show that the ordered state below 6.7 K is a canted antiferromagnet and consists of large antiferromagnetic  $ac$ -components and smaller ferromagnetic  $b$ -components. By first-principle calculations and linear spin wave analysis, we present a simple spin hamiltonian with non-uniform nearest neighbor exchange interactions resulting in a system of coupled spin trimers with a single-ion anisotropy that can qualitatively reproduce the spin dynamics of  $\text{Cu}_2(\text{OD})_3\text{Cl}$ .

PACS numbers: 75.10.Jm, 75.25.+z, 75.50.Ee

The quest for novel quantum spin states in a space higher than one-dimension has been active [1] since the resonating valence bond state was proposed as the ground state of a two-dimensional quantum spin triangular system [2] and was also proposed to be relevant to high  $T_c$  superconductivity in cuprates [3]. Recently, a few compounds have attracted lots of attention as good model systems [4]. One of them is  $\text{Cu}_{4-x}\text{Zn}_x(\text{OD})_6\text{Cl}_2$  which was initially believed to realize a two-dimensional kagome lattice with quantum spins when  $x = 1$  and a three-dimensional pyrochlore when  $x = 0$ . [5] The prospect looked promising because  $\text{Cu}_{4-x}\text{Zn}_x(\text{OD})_6\text{Cl}_2$  does not order down to 50 mK for most values of  $x$ . [6]

Recent neutron diffraction studies, however, have found that  $\text{Cu}_3\text{Zn}(\text{OD})_6\text{Cl}_2$  with rhombohedral  $R\bar{3}m$  symmetry realizes a perfect kagome lattice but with 10% nonmagnetic site disorder. [7, 8] Furthermore, when Zn ions are replaced by Cu ions,  $\text{Cu}_{4-x}\text{Zn}_x(\text{OD})_6\text{Cl}_2$  with  $x < 0.3$ , becomes monoclinic ( $P2_1/n$ ) due to the Jahn-Teller effects of  $\text{Cu}^{2+}(3d^9)$  ion. This leads to different bond angles for different Cu-O-Cu superexchange paths in such a way that the kagome lattice is distorted to have nonuniform nearest neighbor interactions and the interplane coupling between the kagome and triangular planes is expected to be weak. Thus  $\text{Cu}_{4-x}\text{Zn}_x(\text{OD})_6\text{Cl}_2$  realizes a good two dimensional quantum spin system for all  $x$  but it does have defects with regards to an ideal kagome quantum antiferromagnet: for  $x = 1$  the nonmagnetic site disorder while for  $x = 0$  the nonuniform coupling constants. [7]

The distorted kagome quantum spin system  $\text{Cu}_2(\text{OD})_3\text{Cl}$  is interesting in its own right. Specific heat measurements have shown that upon cooling it undergoes two transitions, one at  $T_{c2} = 18$  K and another at  $T_{c1} = 6.7$  K. [9] Muon spin relaxation ( $\mu\text{SR}$ ) measurements yielded evidence for long range order at  $T_{c2}$  and for enhancement of strong spin fluctuations

at  $T_{c1}$ . [9, 10] However, in the specific heat data the amount of entropy given off at the  $T_{c2}$  transition is tiny in comparison to the change in entropy at  $T_{c1}$ , which appears inconsistent with the  $\mu\text{SR}$  results. Neutron diffraction studies revealed development of observable magnetic Bragg peaks only below  $T_{c1}$  [7], which indicates that this transition is associated with Néel order, a result that is consistent with the large amount of entropy released at  $T_{c1}$  but not at  $T_{c2}$ . The spin structure was found to be collinear rather than the  $120^\circ$  configuration that is expected for a uniform kagome antiferromagnet. A recent theoretical study showed that collinear spin structures can indeed be favored by a distorted kagome. [11] For  $T_{c1} < T < T_{c2}$ , on the other hand, there were no observable magnetic peaks but instead a weak magnetic excitation was observed at an energy transfer  $\hbar\omega = 7$  meV. [7] This intermediate phase was proposed to be a quantum spin singlet state, in contradiction with the  $\mu\text{SR}$  results.

Here we present our bulk magnetization and neutron scattering measurements on  $\text{Cu}_2(\text{OD})_3\text{Cl}$  under an external magnetic field. Our principal results are the following. (1) The long-range magnetic order below 6.7K consists of strong antiferromagnetic collinear  $ac$ -components ( $|\langle M \rangle_{ac}| = 0.56(10) \mu_B/\text{Cu}^{2+}$ ) and a weak ferromagnetic  $b$ -component ( $|\langle M \rangle_b| = 0.151 \mu_B/\text{Cu}^{2+}$ ). (2) The 7 meV peak in the magnetic excitation spectrum, that was previously ascribed to a quantum singlet state, is due to a van Hove singularity of the spin wave excitations at the zone boundary of the excitation spectrum. (3) The spin dynamics can be qualitatively explained by a simple spin hamiltonian with non-uniform nearest neighbor exchange interactions resulting in three different coupling constants with values of 8 meV, 3.7 meV and 2.8 meV in the kagomé plane and a single ion anisotropy of 0.4 meV.

A 20 g powder sample of  $\text{Cu}_2(\text{OD})_3\text{Cl}$  was made at the University of Fukui using the standard method re-

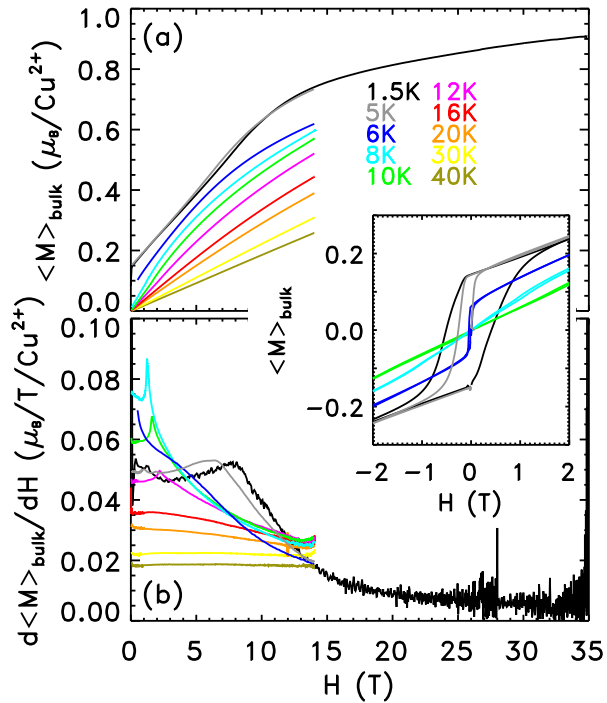


FIG. 1: (a) Bulk magnetization,  $\langle M \rangle_{bulk}$ , and (b) susceptibility,  $d\langle M \rangle_{bulk}/dH$ , measured as a function of an external magnetic field at several different temperatures. The inset shows the low field ( $-2 \text{ T} < H < 2 \text{ T}$ ) data of  $\langle M \rangle_{bulk}$  at five selected temperatures.

ported elsewhere.[5] Bulk magnetization measurements up to  $H = 12 \text{ T}$  were performed at the Hahn-Meitner Institut (HMI), Berlin, while high field measurements up to  $H = 35 \text{ T}$  were done at the IMR, Tohoku University. Neutron scattering measurements were performed at the NIST Center for Neutron Research (NCNR) and at the Berlin Neutron Scattering Center (BENS) at HMI. Details of the neutron scattering experimental setups are described in the captions of the figures that present the data.

Fig. 1 (a) shows bulk magnetization,  $\langle M \rangle_{bulk}$ , measured as a function of an external magnetic field,  $H$ , at various temperatures, spanning the two phase transitions at  $T_{c1} = 6.7 \text{ K}$  and  $T_{c2} \sim 20 \text{ K}$ . At  $T = 1.5 \text{ K} \ll T_{c1}$ ,  $\langle M \rangle_{bulk}$  has a nonzero value of  $0.15 \mu_B/\text{Cu}^{2+}$  at  $H = 0 \text{ Tesla}$  and exhibits hysteresis with  $H$  (see inset). This tells us that the Néel state below  $T_{c1}$  has ferromagnetic components. As shown in Fig. 2 (a), below  $T_{c1}$ , antiferromagnetic Bragg reflections with the characteristic wave vector of  $\mathbf{Q}_m = (0,0,0)$  appear. The ferromagnetic component clearly observed in  $\langle M \rangle_{bulk}$  would yield magnetic scattering on the top of the nuclear Bragg reflections only. We have applied the group theoretical approach in solving the magnetic structure. There are four irreducible representations of group  $P2_1/n$  for  $\mathbf{Q}_m$ . Among

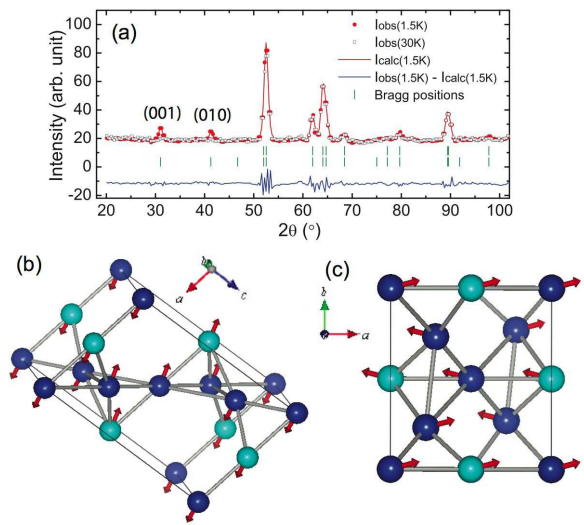


FIG. 2: (a) Elastic neutron scattering as a function of the scattering angle,  $2\theta$ . The spin structure projected (b) on the  $ac$ -plane and (c) on the  $ab$ -plane. Blue and green spheres in (b) and (c) represent kagomé and triangular  $\text{Cu}^{2+}$  spins, respectively.

them, the representation  $\tau_1$  has antiferromagnetic basis functions for the crystallographic  $a$ - and  $c$ -components,  $\psi_{\tau_1}^a = (1, 0, 0)$  and  $\psi_{\tau_1}^c = (0, 0, 1)$ , respectively, and ferromagnetic  $b$ -component,  $\psi_{\tau_1}^b = (0, 1, 0)$ . We have found that the linear combination of the basis functions of the  $\tau_1$  representation,  $0.55(5)\psi_{\tau_1}^a + 0.151\psi_{\tau_1}^b + 0.23(25)\psi_{\tau_1}^c$ , reproduces our elastic neutron scattering pattern (Fig. 2 (a)). As shown in Fig. 2 (b), the  $ac$ -components form the collinear, antiferromagnetic spin arrangement that was proposed previously. [7]

When an external magnetic field is applied up to about 10 Tesla,  $\langle M \rangle_{bulk}$  increases rapidly to the average value of  $0.7 \mu_B/\text{Cu}^{2+}$ . For  $H > 10 \text{ Tesla}$ ,  $\langle M \rangle_{bulk}$  keeps increasing at a slower rate to  $0.9 \mu_B/\text{Cu}^{2+}$  at  $H = 35 \text{ Tesla}$  which is close to the value of  $1 \mu_B/\text{Cu}^{2+}$ , expected when all spins are fully polarized ferromagnetically. The change in the increase rate can also be seen in  $d\langle M \rangle_{bulk}/dH$  vs  $H$  (Fig. 1 (b)) which exhibits a broad peak at around  $H = 8 \text{ Tesla}$  and decreases rapidly at higher  $H$ , indicating a field-induced magnetic phase transition. Upon warming, the antiferromagnetic  $ac$ -components weaken[7], and so does the ferromagnetic  $b$ -component (see the 6 K data in the inset), and both components disappear at  $T_{c1} = 6.7 \text{ K}$ [5, 7]. At  $T = 6 \text{ K} \sim T_{c1}$ , the broad peak which was found in  $d\langle M \rangle_{bulk}/dH$  at  $H_{c1} \sim 8 \text{ Tesla}$  at  $T \ll T_{c1}$  becomes a broader bump at a lower  $H_{c1} \sim 5 \text{ Tesla}$ . While in the intermediate phase,  $T_{c1} < T < T_{c2}$ , the broad peak found in  $d\langle M \rangle_{bulk}/dH$  for  $T < T_{c1}$  is now replaced by a sharp peak at low  $H$ ;  $H_{c2} = 1.5, 2, 2.2 \text{ Tesla}$  for  $T = 8, 10, 12 \text{ K}$ , respectively, and at  $16 \text{ K}$  a broad peak at around  $H_{c2} = 2 \text{ Tesla}$ . At  $30 \text{ K}$  and  $40 \text{ K} > T_{c2}$ ,  $d\langle M \rangle_{bulk}/dH$  is

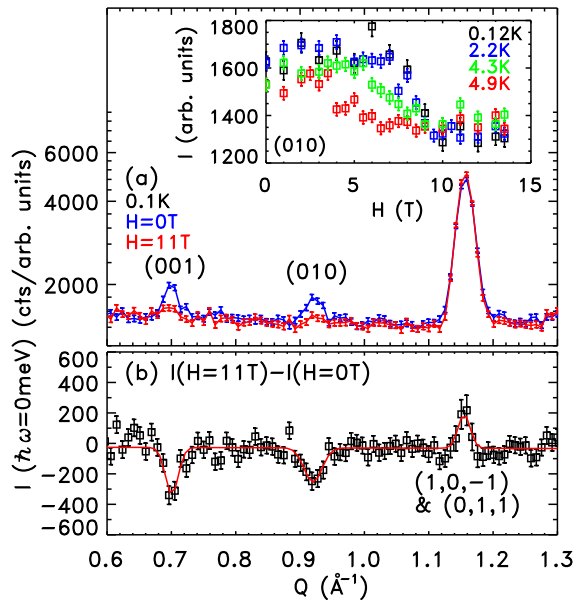


FIG. 3: (a) Elastic neutron scattering pattern as a function of  $Q$  up to  $1.3 \text{ \AA}^{-1}$ , obtained at  $T = 0.1 \text{ K}$  under an external magnetic field of  $0 \text{ T}$  (blue) and  $3.5 \text{ T}$  (red). (b) The difference between the two diffraction pattern,  $I(H = 11 \text{ T}) - I(H = 0 \text{ T})$ . The data were obtained with an incident neutron energy of  $E_i = 3.7 \text{ meV}$  and collimation of guide-80-80-open at the cold-neutron triple-axis spectrometer, SPINS, located at the NCNR. Contamination from higher-order neutrons were eliminated by placing a BeO filter after the sample. Inset of (a): H-dependence of the (010) Bragg peak intensity at four different temperatures,  $T = 0.12 \text{ K}$ ,  $2.2 \text{ K}$ ,  $4.3 \text{ K}$  and  $4.9 \text{ K}$ . The measurements were done at the cold neutron triple-axis spectrometer V2 at HMI with  $E_i = 5 \text{ meV}$ .

nearly flat, i.e.,  $\langle M \rangle_{bulk}$  increases linearly with  $H$ , up to  $H = 14 \text{ Tesla}$ , suggesting paramagnetic behaviour.

To study the field effects on the Neel state below  $T_{c1}$ , we have performed elastic neutron scattering measurements with an external magnetic field. Fig. 3 (a) shows the elastic neutron scattering pattern as a function of momentum transfer,  $Q$ , measured at  $T = 0.12 \text{ K}$  with two different fields,  $H = 0 \text{ T}$  (blue symbols) and  $11 \text{ T}$  (red symbols). The two antiferromagnetic Bragg peaks at the (001) and (010) reflections, that are prominent in zero field, become very weak at  $H = 11 \text{ T}$ , indicating a field induced phase transition occurred below  $H = 11 \text{ T}$ . The inset of Fig. 3 (a) shows that at  $T = 0.12 \text{ K}$  the peak starts weakening at around  $7 \text{ T}$  which is close to the  $H_{c1} = 8 \text{ T}$  observed in  $d\langle M \rangle_{bulk}/dH$  and disappears at around  $10 \text{ T}$ . When temperature increases, the critical field decreases, for instance  $H_{c1} = 6.5 \text{ T}$  at  $T = 4.9 \text{ K}$ , which is consistent with our bulk magnetization data. Where did the antiferromagnetic scattering go? The intensity difference between  $H = 0$  and  $11 \text{ T}$ , plotted in Fig. 3 (b), shows that the peak at  $Q = 1.16 \text{ \AA}^{-1}$  which corresponds to the nuclear (1,0,-1) & (0,1,1) reflections has

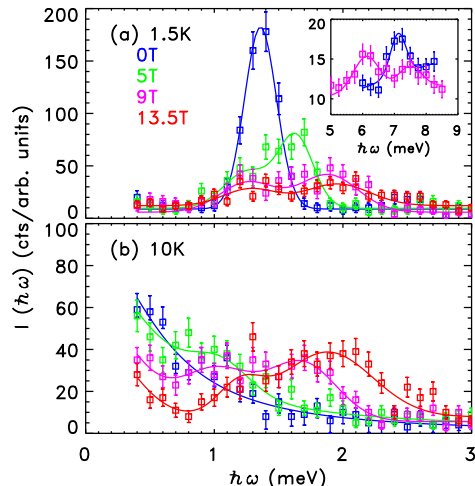


FIG. 4: Inelastic neutron scattering intensity obtained at  $Q = 0.6 \text{ \AA}^{-1}$  under external magnetic fields of,  $H = 0 \text{ T}$  (blue),  $5 \text{ T}$  (green),  $9 \text{ T}$  (pink) and  $13.5 \text{ T}$  (red), at temperatures of  $T = 1.5 \text{ K}$  (a) and  $10 \text{ K}$  (b). The data were obtained at the cold-neutron triple-axis spectrometer V2. The data shown in the inset of (a) were obtained at  $Q = 1.2 \text{ \AA}^{-1}$ , at the SPINS. At both spectrometers, the energy of the scattered neutrons was fixed to be  $E_f = 3.7 \text{ meV}$  and a horizontally focusing analyzer was utilized to increase the sensitivity.

increased upon application of the field. Altogether, the neutron and susceptibility data suggest a picture where below  $8 \text{ T}$  the field increases the size of the spin moment without changing its direction significantly. In contrast, above  $8 \text{ T}$  where the ferromagnetic component increases at the expense of the antiferromagnetic component and the spins are able to increase their alignment with the field perhaps by overcoming an anisotropy.

Let us now turn to field effects on spin fluctuations. Fig. 4 (a) shows the H-dependence of the magnetic excitation spectrum measured at  $T = 1.5 \text{ K} \ll T_{c1}$ . At  $H = 0 \text{ Tesla}$ , there are two modes centered at  $\hbar\omega = 1.32 \text{ meV}$  and  $7 \text{ meV}$ , as previously reported [7]. When  $H$  is applied, the sharp peak at  $1.3 \text{ meV}$  splits into two broad peaks and the splitting between the two peaks increases with  $H$ . At  $H = 13.5 \text{ T}$ , the two peaks are centered at  $\hbar\omega = 1.25 \text{ meV}$  and  $2 \text{ meV}$ , respectively. The  $7 \text{ meV}$  peak also splits into two peaks (see inset), which unambiguously tells us that it is not due to the singlet-to-triplet excitations of a quantum dimer as previously thought, but is due to spin waves. At  $10 \text{ K} > T_{c1}$ , and zero field, the  $\hbar\omega = 1.3 \text{ meV}$  mode is replaced by a low energy continuum (see Fig. 4 (b)), commonly found in a cooperative paramagnet. When the magnetic field is applied, distinct excitation modes appear out of the continuum. For  $H \geq 9 \text{ T}$ , there exist a broad feature that can be fitted by two gaussians. At  $H = 13.5 \text{ T}$ , the two peaks are centered at  $1.25 \text{ meV}$  and  $2 \text{ meV}$ . This behavior is quite different

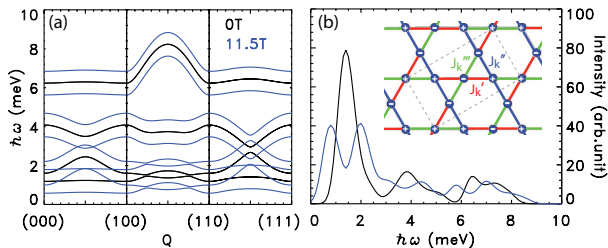


FIG. 5: (a) Dispersion of spin wave excitations along  $(h,0,0)$ ,  $(1,k,0)$ , and  $(1,1,l)$  directions. (b) Powder-averaged neutron scattering intensity as a function of  $\hbar\omega$ . Black and blue lines are the results for  $H = 0$  T and 11.5 T, respectively. The inset of (b) shows the kagomé lattice with the  $ac$ -components of the moments. Red, blue, green lines represent different bond strengths.

from the field-induced single-ionic Zeeman-like behavior observed in  $\text{Cu}_{4-x}\text{Zn}_x(\text{OD})_6\text{Cl}_2$  ( $x=0.66$  and  $1$ ) [6, 7]. Instead, it is very similar to the behavior observed at 1.5 K (see Fig. 4 (a)) in an external field. This indicates that the paramagnetic continuum at low energies above  $T_{c1}$  is due to spin fluctuations anticipating the canted antiferromagnetic order below  $T_{c1}$ . This also suggests that the 7 meV mode that survives above  $T_{c1}$  might be related to the spin wave fluctuations of the Néel state.

It is almost impossible to extract the exact spin hamiltonian,  $\mathcal{H}$ , from powder-averaged inelastic neutron scattering data, because the crystallographic directional information is lost. This is especially the case when  $\mathcal{H}$  is complex as in  $\text{Cu}_2(\text{OD})_3\text{Cl}$ . Therefore we have performed the local-density approximation (LDA)+ $U$  (the  $d-d$  Coulomb interaction parameter) calculations for a wide range of  $U$  to obtain the ratios of different exchange constants. Our results tell us that there are three different coupling constants in the kagomé plane as shown in the inset of Fig. 5b with the ratios of  $J_k''/J_k' \simeq 0.46$  and  $J_k'''/J_k' \simeq 0.35$ . [12] The inter-plane couplings turned out to be much weaker, less than  $0.1J_k'$ . We then performed linear spin wave analysis with those ratios fixed and with two fitting parameters,  $J_k'$ , that couples the spins into trimers, and a single ion anisotropy along the spin direction,  $D$ , for the collinear AFM structure composed of the  $ac$ -components of the  $\text{Cu}^{2+}$  ions, neglecting the FM  $b$ -components.

We focused on the following experimental observations: upon warming the 1.3 meV mode shifts to lower energies as the frozen moment weakens while the 7 meV mode does not shift in energy. [7] This suggests that the 1.3 meV excitation is a zero energy mode shifted to finite energy by anisotropy, while the 7 meV mode is due to the van Hove singularity of the excitations at the zone boundary of the excitation spectrum. As shown in Fig. 5 (b), a sharp and strong peak at 1.3 meV and a weak

and broad peak at 7 meV can be generated in zero field with  $J_k' = 8$  meV and  $D = -0.4$  meV. Fig. 5 (a) show that the 1.3 meV peak is due to two nearly-flat doubly generate modes, while the 7 meV peak arises from the enhanced density of states at the zone-boundary energy of another doubly degenerate mode. The fourth doubly degenerate mode generates two broad peaks around 4 meV, which have not been observed experimentally. The discrepancy may tell us that the exchange interactions are not isotropic or the asymmetric exchange interactions such as the Dzyaloshinskii-Moriya interactions need to be included in our analysis.

When a Zeeman term,  $g\mu_B H \cdot \sum S_i^a$ , is included in the spin hamiltonian, the 1.3 meV peak splits into two peaks at a lower and a higher energy, while the excitations around 7 meV becomes broader and exhibit two peaks at around 6 meV and 7 meV, which are qualitatively consistent with the data shown in Fig. 4 (a). Thus, the previous interpretation of the 7 meV excitation as a triplet associated with spin dimers in the intermediate temperature ( $6.7 \text{ K} < T < 18 \text{ K}$ ) regime [7] should be modified to reflect the large intratrimer interactions. So far, the observed characteristics of this phase are the weak anomaly in the specific heat,  $\mu\text{SR}$  measurements, and the small kinks in our  $d\langle M \rangle_{\text{bulk}}/dH$  vs  $H$  data. Further experimental and theoretical investigations are necessary to understand the nature of the intermediate T phase.

In summary, using bulk susceptibility, and elastic and inelastic neutron scattering measurements with and without an external magnetic field, we have characterized the static and dynamic spin correlations in  $\text{Cu}_2(\text{OD})_3\text{Cl}$ . Our analysis shows that  $\text{Cu}_2(\text{OD})_3\text{Cl}$  should be considered as a system of coupled spin trimers on the kagomé lattice.

We thank A. B. Harris, S. Nagler, T. J. Sato, Y. B. Kim, M. Kofu for helpful discussion.

- 
- [1] S. Sachdev, Nat. Phys. **4**, 173 (2008) and references therein.
  - [2] P. Fazekas and P. W. Anderson, Philos. Mag. **30**, 423 (1974).
  - [3] P. W. Anderson, Science **235**, 1196 (1987).
  - [4] B. G. Levi, Physics Today **60**, 16 (2007); Y. Shimizu *et al.*, Phys. Rev. Lett. **91**, 107001 (2003); S. Nakatsuji *et al.*, Science **309**, 1697 (2005); O. I. Motrunich, Phys. Rev. B **72**, 045105 (2005).
  - [5] M. P. Shores *et al.*, J. Am. Chem. Soc. **127**, 13462 (2005).
  - [6] J. S. Helton *et al.*, Phys. Rev. Lett. **98**, 107204 (2007).
  - [7] S.-H. Lee *et al.*, Nat. Mat. **6**, 853 (2007).
  - [8] M. A. de Vries *et al.*, Phys. Rev. Lett. **100**, 157205 (2008).
  - [9] X. G. Zheng *et al.*, Phys. Rev. B **71**, 052409 (2005); Phys. Rev. Lett. **95**, 057201 (2005).
  - [10] P. Mendels *et al.*, Phys. Rev. Lett. **98**, 077204 (2007).

- [11] M. J. Lawler *et al.*, Phys. Rev. Lett. **100**, 187201 (2008).
- [12] T. Yildirim *et al.*, in preparation (2008).